H-mode Scrape-Off Layer power width in the TCV tokamak

R. Maurizio,[1, a)] B.P. Duval,[1] B. Labit,[1] H. Reimerdes,[1] M. Faitsch,[2] M. Komm,[3] U. Sheikh,[1] C. Theiler,[1] the TCV Team,[4] and the EUROfusion MST1 Team[5]

[1)] *École Polytechnique Fédérale de Lausanne (EPFL), Swiss Plasma Center (SPC), CH-1015 Lausanne, Switzerland*

[2)] *Max-Planck-Institute for Plasma Physics, Boltzmannstr. 2, D-85748 Garching, Germany*

[3)] *Institute of Plasma Physics of the CAS, Za Slovankou 3, 182 00 Prague 8, Czech Republic*

[4)] *See author list of "S. Coda et al Nucl. Fusion 59 (2019) 112023"*

[5)] *See author list of "B. Labit et.al. Nucl. Fusion 59 (2019) 086020"*

(Dated: 11 November 2020)

Abstract Obtaining acceptable conditions at the divertor targets of a next-step fusion experiment based on the tokamak concept is expected to be particularly challenging because of the small predicted value of the plasma power exhaust channel width. An increased confidence in this prediction is important to forestall any power exhaust issue and in developing corresponding divertor solutions. With the present prediction relying on empirical scaling laws based on data from six tokamaks, this letter tests these scaling laws on an additional device, the TCV tokamak. Estimates of the exhaust channel width, λ_q, based on Thomson scattering measurements of the electron temperature and density profiles, correlate well with outer target infrared thermography. Reasonable agreement with multi-device scaling laws is found only when including both the power crossing the separatrix and the Greenwald density fraction as regression parameters. TCV's λ_q is 2 to 3 times smaller than in spherical tokamaks for the same value of the poloidal field. The inclusion of TCV data in the scaling laws would, therefore, require the retention of an explicit aspect ratio dependence, with consequences for all other dependencies.

I. INTRODUCTION

Handling the high plasma power exhaust to the divertor targets of a future nuclear fusion reactor remains a great technological and physics challenge. As the width of the power exhaust channel (known as Scrape-Off Layer, SOL) is projected to be very small, e.g. $\lambda_q \sim 1$ mm for ITER [1], the peak heat flux onto the divertor targets, if unmitigated, will significantly exceed the limit for actively cooled surfaces. Acceptable target conditions, i.e. sufficiently low plasma heat flux and temperature at the targets, only become possible with the divertor in the detached regime. Access to this regime may be particularly challenging in a fusion reactor, as the plasma density (or the density of a low-Z impurity, used as a divertor radiator) needed to detach the divertor increases for decreasing λ_q. An accurate prediction of λ_q in a future fusion reactor becomes critical to forestall in time any potential problems and develop alternative divertor solutions. The present λ_q prediction [1] derives from scaling laws developed using divertor target infrared thermography measurements on six tokamaks, which vary in size, magnetic field strength and aspect ratio.

This letter tests these scalings on the TCV tokamak [2], where plasmas have geometric major radius $R_{\rm geo} = 0.88$ m, toroidal magnetic field, at $R_{\rm geo}$, $B_\phi = 1.42$ T and plasma aspect ratio $R_{\rm geo}/a = 4$ (a is the plasma minor radius). TCV, thereby, adds a different combination of these key configuration parameters to the devices that contributed to the scalings. Section II describes the diagnostic methods to estimate λ_q. Section III discusses the measurements of λ_q as the plasma transitions from a L- to an ELM-free H-mode, comparing, in particular, estimates from Thomson scattering and infrared thermography systems. Section IV focuses on the λ_q of ELMy H-mode plasmas, with a comparison to the predictions of multi-device regressions, revealing important disagreements. Some discussion and conclusions are presented in section V.

II. EXPERIMENTAL METHODS

Measurements of λ_q on TCV are performed using infrared (IR) thermography and Thomson scattering (TS). The infrared thermography system [3] measures divertor target heat load profiles, with a typical integration time of ~ 1 ms and sampling frequency of 200 Hz, which must be decreased to ~ 0.1 ms and a few kHz for plasmas exhibiting ELMs. The heat load profiles are mapped to the plasma outboard mid-plane using the magnetic reconstruction and fitted with the functional form proposed in [4] to estimate λ_q. The Thomson scattering system measures the electron temperature and density profiles at the plasma core and edge, with an integration time of 10 ns and a sampling frequency of 60 Hz [5], which are appropriate for inter-ELM measurements. These profiles are mapped to the plasma outboard mid-

[a)] Current address: General Atomics, San Diego, 92186 CA, USA; Electronic mail: maurizior@fusion.gat.com

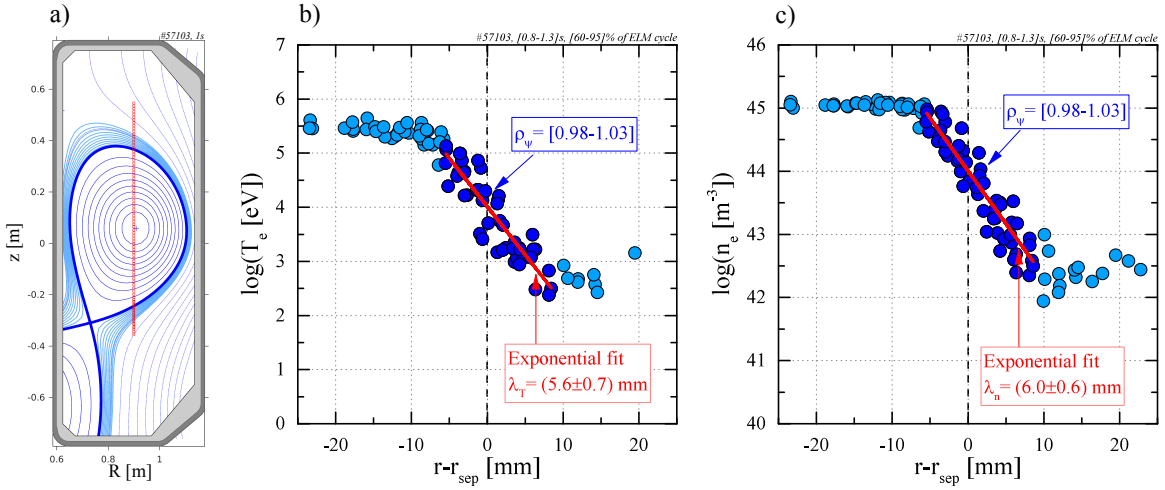

FIG. 1. (a) Poloidal cross-section of TCV vessel, showing a typical Single-Null equilibrium (blue) and the emitting volumes of the Thomson Scattering system (red). (b-c) Profiles of plasma electron temperature (b) and density (c) near the magnetic separatrix, of the magnetic equilibrium shown in (a), as a function of the radial distance from the separatrix at the plasma outboard mid-plane. Only measurements below the magnetic axis are considered. Both profiles are fitted with an exponential function (red) in the edge region ($0.98 \leq \rho_\psi \leq 1.03$, with ρ_ψ the normalized poloidal flux coordinate, shown in dark blue). This plasma is an ELMy H-mode and the TS profiles describe the inter-ELM phase (60 to 95 % of the ELM cycle). The exponential fit interval is chosen in such a way as to exclude the plasma pedestal and the far-SOL region.

plane using the magnetic reconstruction, and are fitted with an exponential function in the edge region to estimate their fall-off lengths λ_T and λ_n, see figure 1, similarly to [6–8]. The fit is limited to the interval $0.98 \leq \rho_\psi \leq 1.03$, with ρ_ψ being the normalized poloidal flux coordinate, corresponding to a radial distance from the separatrix at the plasma outboard mid-plane of approximately -8 mm $\leq r - r_{\rm sep} \leq 9$ mm. Since the plasma profiles do not show clear signs of change of slope at the separatrix, the fit interval can be reasonably extended inside the separatrix, up to (but excluding) the pedestal region, where the slope changes. In the SOL, the fit interval is limited at $\rho_\psi \approx 1.03$ to exclude the typical broadening of the profiles in the far-SOL. Note that the fitting procedure only uses measurements below the magnetic axis, due to a detectable radial shift between measurements below and above the magnetic axis that is occasionally observed. Such a shift arises from small poloidal gradients in the plasma parameters but can also be affected by uncertainties in the reconstruction of plasma position and elongation. Using data from only one side avoids an artificial broadening of the profiles. This may result in a systematic error of the separatrix position but not of the plasma profile gradients, which are not sensitive to the exact location of the fitting interval (as discussed above).

The link between λ_T, λ_n and λ_q is expected to depend on the SOL transport regime [9]. If parallel energy transport in the SOL is dominated by Spitzer (collisional) parallel heat conduction of electrons, λ_q is approximated by

$$\lambda_q^{\rm Spitzer} = \frac{2}{7}\lambda_T \qquad (1)$$

In the opposite extreme of weak collisionality, parallel energy transport is sheath-limited, i.e. parallel gradients of T_e are negligible. For intermediate collisionality, the Spitzer conductivity is flux-limited and is modified using a 'kinetic correction'([9,11] and Secs. 4.1–26.2 of [10]); λ_q is then approximated by

$$\lambda_q^{\text{flux-limited}} = \left(\frac{3/2}{\lambda_T} + \frac{1}{\lambda_n}\right)^{-1} \qquad (2)$$

In section III, these two λ_q estimates are compared with those measured by IR at the divertor targets.

III. ELM-FREE H-MODE

The values of λ_q estimated by TS are compared to target IR measurements with the plasma in the L-mode and ELM-free H-mode, since, in these confinement regimes, both diagnostics yield a high signal amplitude. In the absence of ELM heat transients, a longer integration time for the IR system can be chosen, providing a stronger signal at the divertor targets. For a standard lower Single-Null magnetic configuration, with the ion vertical $B\times\nabla B$ drift towards the active x-point, and a plasma current of 320 kA, a transition from L- to ELM-free H-mode is induced by adding $\approx$ 200 kW of neutral beam power. The transition is identified by a sharp decrease in the D_α-line intensity (see top of figure 2), an increase in the plasma line-averaged density, a steepening of the edge plasma electron density and temperature profiles that show the formation of a pedestal inside the separatrix. The transition to H-mode is accompanied by a narrowing of the divertor target heat flux profiles.

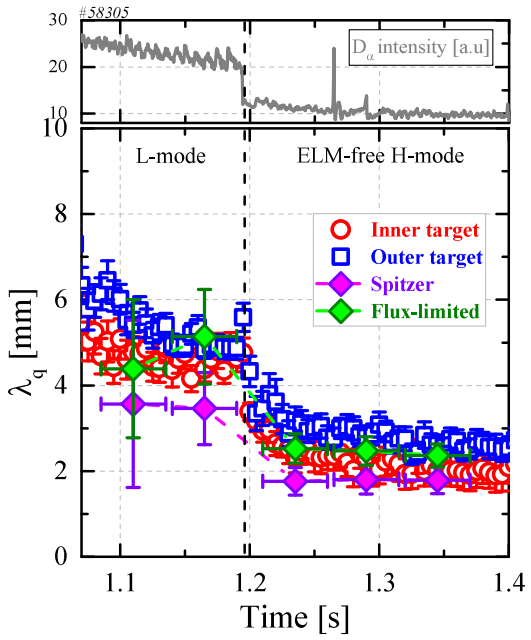

FIG. 2. (Top) Time evolution of D_α line intensity, with a sharp drop at ≈1.2 s indicating the transition from L- to ELM-free H-mode. (Bottom) Time evolution of λ_q values inferred from target infrared thermography (blue squares for outer divertor target, red circles for inner divertor target) and upstream Thomson scattering (green diamonds if using the flux-limited expression for λ_q, purple diamonds if using the Spitzer formula). Each TS data point corresponds to 3 TS measurements, within a 50 ms time interval.

With the plasma in ELM-free H-mode, λ_q estimated by TS with the low-collisionality assumption, equation 2, agrees well with that from IR at the outer target, figure 2, although it may systematically underestimate it by $\sim 10\%$. Note that, despite this correlation, one cannot conclude that the SOL is in the flux-limited regime, since equations 1-2 are based on simple models that neglect other effects that broaden the target heat flux profiles, e.g. the radiation load. The SOL collisionality can be computed with $\nu^*_{\rm SOL} \approx 10^{-16} n_{e,u} L_\parallel / T^2_{e,u}$ [10], where $n_{e,u}$ and $T_{e,u}$ are the separatrix electron density and temperature, measured at the outboard mid-plane with TS, and $L_\parallel$ the magnetic field line length from the outboard mid-plane to the outer divertor plate (averaged across the SOL in the vicinity of the separatrix: $0\ {\rm mm} \leq r - r_{\rm sep} \leq 2\ {\rm mm}$). This yields $\nu^*_{\rm SOL} \approx 14$, indicating moderate SOL parallel temperature gradients.

The factor 2 decrease of target λ_q at the transition from L- to ELM-free H-mode agrees well with observations from the JET tokamak, where the outer divertor λ_q also decreases by a factor 2 [12], and is more generally observed also at the transition from L- to ELMy H-mode [7,13]. On TCV, the decrease of λ_q at both targets can be entirely attributed to the decrease of λ_q at the outboard mid-plane.

Parameter	Range	Parameter	Range
$I_{\rm P}$ [MA]	0.17–0.38	$f_{\rm GW}$	0.23–0.55
q_{95}	2.02–4.73	$\delta_{\rm upper}$	0.08–0.61
$P_{\rm SOL}$ [MW]	0.57–1.60	$\delta_{\rm lower}$	0.52–0.74
$B_{\rm pol}$ [T]	0.16–0.31	$f_{x,t}$	1.9–8.7

TABLE I. Overview of explored parameter range for ELMy H-mode plasmas on TCV.

IV. H-MODE WITH TYPE-I ELMS

The TCV database considered for this work features 20 H-mode discharges exhibiting type-I ELMs, in a standard lower Single-Null configuration with the ion vertical $B \times \nabla B$ drift from the core towards the active x-point. Both divertors are, again, in the attached regime as target Langmuir probes measure inter-ELM electron temperatures up to ≈ 20 eV (e.g. for the plasma shot of figure 1 , the outer strike point temperature is 18 eV). The line-averaged plasma density is kept below 55% of the Greenwald density.

An overview of the explored range of plasma and magnetic parameters is provided in Table I. The parameters are: q_{95}, the safety factor at the 95% poloidal flux surface, $P_{\rm SOL} = P_\Omega + P_{\rm NBI} + P_{\rm ECH} - P_{\rm rad,core}$, the power crossing the separatrix and entering the SOL, $B_{\rm pol}$, the poloidal magnetic field strength at the outboard mid-plane (from magnetic reconstruction), $f_{\rm GW}$, the Greenwald density fraction, $\delta_{\rm upper}$/ $\delta_{\rm lower}$, the plasma upper / lower triangularity, and $f_{x,t}$, the outer target flux expansion. Note that the ELM-free shot of section III is well representative of this ELMy database, with, at t=1.35 s, $I_{\rm P}$ =0.32 MA, q_{95} =2.39, $P_{\rm SOL}$ =1.6 MW, $B_{\rm pol}$ =0.27 T, $f_{\rm GW}$ =0.6, $\delta_{\rm upper}$ =0.11, $\delta_{\rm lower}$ =0.55 and $f_{x,t}$ =2.8. The outer divertor leg length $L_{\rm div}$, defined as the vertical distance between x-point and target, is approximately constant over the chosen discharges, ranging from 43 to 51 cm (as a reference, the equilibrium of figure 1a has $L_{\rm div}$ = 44 cm). Note that the ratio of $L_{\rm div}$ and the plasma vertical elongation in TCV is higher than in the tokamaks of [1]. The discharges use a neutral beam injector (NBI), with a power between 0.2 and 1.1 MW, and a second harmonic electron cyclotron heating system (ECH), with powers up to 0.7 MW.

Target IR measurements show that, for the entire database, inter-ELM divertor target heat loads are relatively low, making it difficult to obtain reliable estimates of λ_q. Consequently, λ_q is estimated from Thomson scattering profiles with the flux-limited expression, equation 2. This approach is assumed to be equivalent to outer target IR measurements, as shown in section III. The inter-ELM SOL collisionality, $\nu^*_{\rm SOL} \approx 6$, is even lower than in ELM-free H-mode. For each plasma discharge, the ELMs are detected from their characteristic spikes in the D_α emission, and plasma electron temperature and density profiles from 60 to 95% of the ELM cycles are grouped together, yielding profiles as those shown in fig-

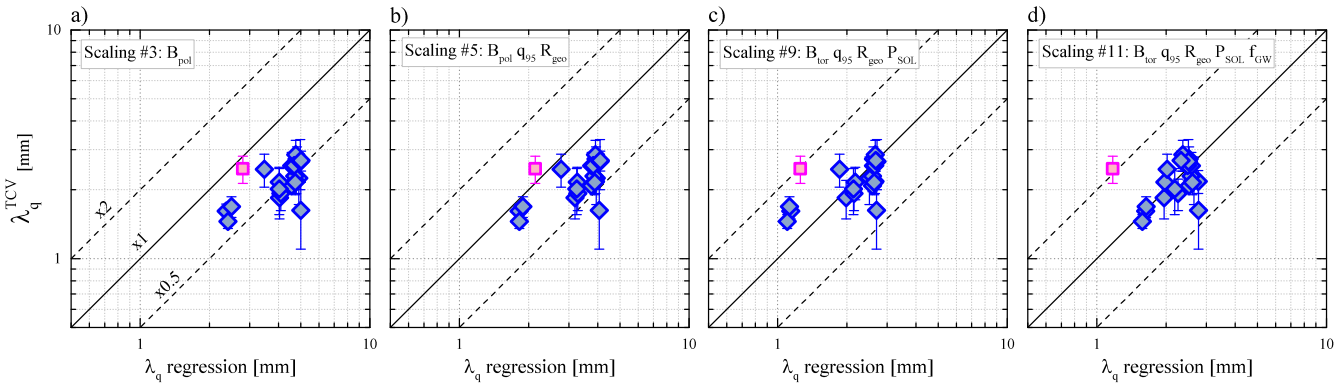

FIG. 3. TCV H-mode λ_q, measured upstream by Thomson scattering using the flux-limited expression 2, for ELMy (blue diamonds) and ELM-free (purple square) plasmas, compared to the prediction from multi-machine regressions based on conventional aspect ratio tokamaks [1]. The regression parameters are indicated inside each figure.

Scaling #	Regression parameters	$\lambda_q^{\rm TCV}/\lambda_q^{\rm scaling}$	RMSE
# 3	$B_{\rm pol}$	(0.53 ± 0.09)	2.137
# 5	$B_{\rm pol}$ q_{95} $R_{\rm geo}$	(0.66 ± 0.13)	1.347
# 9	B_ϕ q_{95} $R_{\rm geo}$ $P_{\rm SOL}$	(1.01 ± 0.22)	0.398
# 11	B_ϕ q_{95} $R_{\rm geo}$ $P_{\rm SOL}$ $f_{\rm GW}$	(0.96 ± 0.15)	0.393
# 14	$B_{\rm pol}$	(0.48 ± 0.09)	2.626
# 15	$B_{\rm pol}$ $R_{\rm geo}$ $P_{\rm SOL}$ $a/R_{\rm geo}$	(0.63 ± 0.09)	1.423

TABLE II. Comparison of TCV H-mode λ_q with the prediction of multi-machine regressions proposed in [1]. Scaling laws #3-5-9-11 are based on conventional aspect ratio tokamaks, while #14-15 include also spherical tokamaks. The Root Mean Square Error (RMSE) is also shown.

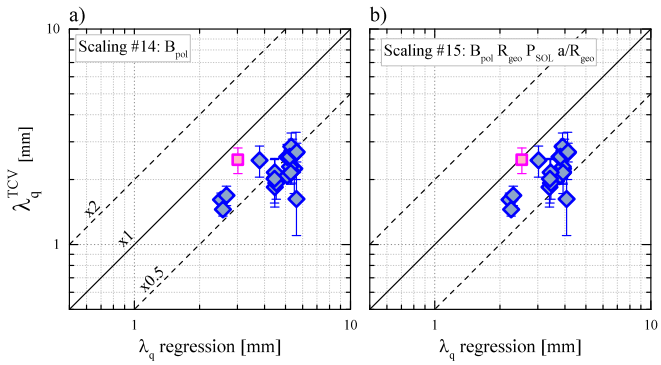

FIG. 4. TCV H-mode λ_q, measured upstream by Thomson scattering using the flux-limited expression 2, for ELMy (blue diamonds) and ELM-free (purple square) plasmas, compared to the prediction from multi-machine regressions based on both conventional and spherical tokamaks [1]. The regression parameters are indicated inside each figure.

ure 1b-c.

The database includes a scan of the outer target flux expansion, from 2.4 to 8.7, with fixed core plasma parameters, at low plasma current (0.17 MA). Increasing the flux expansion has no effect on λ_q, which ranges between 1.6 and 2.2 mm. The effect on λ_q of the remaining parameters of Table I cannot be assessed directly, as more than one parameter is changed at a time.

A comparison of TCV's λ_q with multi-device scaling law predictions [1] is summarized in Table II. The average ratio of measured to predicted value, $\lambda_q^{\rm TCV}/\lambda_q^{\rm scaling}$, is adopted as metric for agreement. Firstly, λ_q is related to the scaling laws #3-5-9-11 in Table 2 of [1], which use data from four conventional aspect ratio tokamaks (JET, DIII-D, AUG, C-Mod). Then, λ_q is related to the scaling laws #14-15 in Table 3 of [1], which use data from the four conventional tokamaks and two spherical tokamaks (NSTX and MAST). The multi-device database includes only experiments with the ion vertical $B \times \nabla B$ drift towards the active x-point, with $R_{\rm geo}$ ranging from 0.7 to 2.95 m, B_ϕ 0.4 to 6.2 T and $R_{\rm geo}/a$ 1.5 to 3.5. TCV extends this regression parameter range to lower plasma currents (from 0.4 MA in MAST to 0.17 MA in TCV), lower safety factors (from 2.6 in AUG to 2.02 in TCV), lower $P_{\rm SOL}$ (from 1 MW in DIII-D to 0.57 MW in TCV) and lower $f_{\rm GW}$ (from 0.3 in MAST to 0.23 in TCV).

For scaling laws based on conventional tokamaks, regressions #3 and #5 significantly overestimate the TCV measurements, figure 3a-b, with $\lambda_q^{\rm TCV}/\lambda_q^{\rm scaling} \approx 0.53$ and ≈ 0.66 respectively. Adding $P_{\rm SOL}$, which is low compared to most cases used for the scaling, as regression parameter, in scaling law #9, improves the agreement with TCV, figure 3c, with $\lambda_q^{\rm TCV}/\lambda_q^{\rm scaling} \approx 1.01$, despite $P_{\rm SOL}$ displaying only a small exponent ($P_{\rm SOL}^{0.09}$). Most notable outliers are measurements at low $f_{\rm GW}$ (≈ 0.23) and high $I_{\rm P}$ (≈ 0.38 MA), visible as three isolated data points on the left of figure 3c . Adding $f_{\rm GW}$ as regression parameter, as in scaling law #11, captures the low $f_{\rm GW}$ cases, figure 3d, yielding good agreement with TCV, with $\lambda_q^{\rm TCV}/\lambda_q^{\rm scaling} \approx 0.96$.

For scaling laws based on conventional and spherical tokamaks (#14-15), both regressions largely overestimate TCV measurements, figure 4a-b, with

$\lambda_q^{\mathrm{TCV}}/\lambda_q^{\mathrm{scaling}} \approx 0.48$ and ≈ 0.63 respectively.

V. DISCUSSION AND CONCLUSIONS

The analysis herein shows that, between the regressions derived for conventional aspect ratio tokamaks, scaling law #11 best reproduces TCV's λ_q, consistently with the ranking found in the publication proposing these regressions [1]. This suggests that λ_q is sensitive to both P_{SOL} and f_{GW} which should, therefore, always be retained as regression parameters in scaling laws for λ_q.

TCV's λ_q is a factor $2-3$ smaller than in spherical tokamaks (MAST and NSTX) for the same value of B_{pol}, figure 5. This difference cannot explained by the different toroidal field ($B_\phi = 0.4$ - 0.5 T in spherical tokamaks, $B_\phi = 1.42$ T in TCV) as the dependence of λ_q on B_ϕ, found for conventional tokamaks, is positive. Considering, for instance, regression #9, and using $q_{95} \propto q_{\mathrm{cyl}} \propto B_\phi$, yields $\lambda_q \propto B_\phi^{-0.77} q_{95}^{1.05} \propto B_\phi^{0.28}$. The strong bifurcation of λ_q at low poloidal field suggests, instead, that λ_q scales positively with the plasma aspect ratio, as already seen in scaling #15 of [1]. However, the disagreement of scaling #15 with TCV measurements clearly indicates that it misses another relevant parameter. The TCV experiments suggest that this parameter could be the Greenwald density fraction f_{GW}. The observed difference between TCV and the spherical tokamaks is consistent with the HD model [14], which predicts a dependence of λ_q on the aspect ratio at fixed poloidal field and separatrix temperature.

The inclusion of spherical tokamaks (MAST and NSTX) in multi-machine regressions, realized in [1] by removing the B_ϕ dependence and increasing the B_{pol} dependence, should, therefore, be revisited. This could be achieved by starting with regression #11, that best describes conventional tokamaks (including TCV), and adding an explicit aspect ratio dependence.

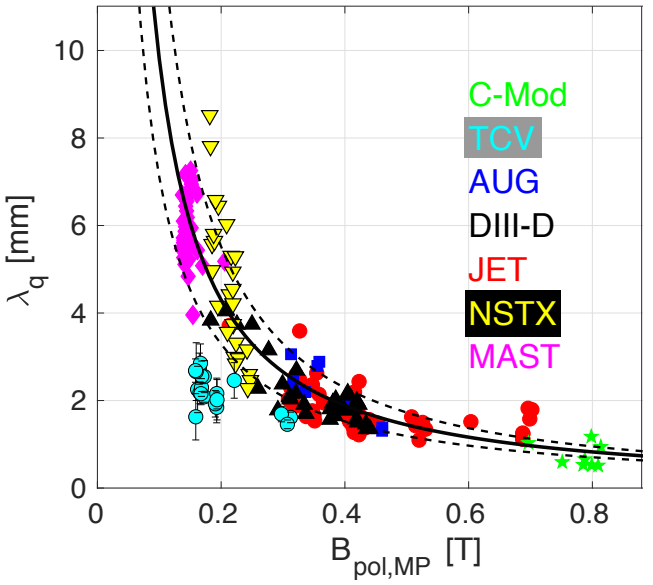

FIG. 5. TCV's ELMy H-mode λ_q, measured upstream by Thomson scattering using the flux-limited expression 2, together with the λ_q from the six tokamaks considered in [1], measured at the outer divertor plate by infrared thermography, as a function of the poloidal field. Scaling law #14 is also shown, $\lambda_q(\mathrm{mm}) = 0.63 \times [B_{\mathrm{pol}}(\mathrm{T})]^{-1.19}$, with its error bars. Adapted from figure 3 of [1].

ACKNOWLEDGMENTS

Very useful and constructive discussions with all members of TCV boundary physics team are truly acknowledged. The authors would like to thank T. Eich for providing the 2013 ITPA λ_q figure. This work was supported in part by the Swiss National Science Foundation. This work has been carried out within the framework of the EUROfusion Consortium and has received funding from the Euratom research and training programme 2014–2018 and 2019–2020 under grant agreement No 633053. The views and opinions expressed herein do not necessarily reflect those of the European Commission.

REFERENCES

[1]Eich T, et al. Scaling of the tokamak near the scrape-off layer H-mode power width and implications for ITER. Nucl Fusion. 2013;53(9):093031. doi: 10.1088/0029-5515/53/9/093031.

[2]Coda S, et al. Overview of the TCV Tokamak Program: Scientific Progress and Facility Upgrades. Nucl Fusion. 2017;57(10):102011. doi: 10.1088/1741-4326/aa6412.

[3]Maurizio R, et al. Divertor power load studies for attached L-mode single-null plasmas in TCV. Nucl Fusion. 2018;58(1):016052. doi: 10.1088/1741-4326/aa986b.

[4]Eich T, et al. Inter-ELM Power Decay Length for JET and ASDEX Upgrade: Measurement and Comparison with Heuristic Drift-Based Model. Phys Rev Lett. 2011;107(21):215001. doi: 10.1103/PhysRevLett.107.215001.

[5]Arnichand H, et al. New capabilities of the incoherent Thomson scattering diagnostics in the TCV tokamak: divertor and real-time measurements. Journal of Instrumentation. 2019;14(09):C09013–C09013. doi: 10.1088/1748-0221/14/09/C09013.

[6]Sun HJ, et al. Study of near scrape-off layer (SOL) temperature and density gradient lengths with Thomson scattering. Plasma Phys Control Fusion. 2015;57(12). doi: 10.1088/0741-3335/57/12/125011.

[7]Sun HJ, et al. Relating the near SOL transport with plasma properties of the confined edge region in ASDEX Upgrade. Plasma Phys Control Fusion. 2019;61(1):014005. doi: 10.1088/1361-6587/aae33c.

[8]Silvagni D, et al. Scrape-off layer (SOL) power width scaling and correlation between SOL and pedestal gradients across L, I and H-mode plasmas at ASDEX Upgrade. Plasma Phys Control Fusion. 2020;62(4):045015. doi: 10.1088/1361-6587/ab74e8.

[9]Stangeby PC, et al. The relation between upstream density and temperature widths in the scrape-off layer and the power width in an attached divertor. Nucl Fusion. 2010;50(12):125003. doi: 10.1088/0029-5515/50/12/125003.

[10]Stangeby PC. The Plasma Boundary of Magnetic Fusion Devices. Institute of Physics Publishing Bristol and Philadelphia; 2000.

[11]Stangeby PC, et al. Identifying the location of the OMP separatrix in DIII-D using power accounting. Nucl Fusion. 2015;55(8):093014. doi: 10.1088/0029-5515/55/9/093014.

[12]Scarabosio A, et al. Outer target heat fluxes and power decay length scaling in L-mode plasmas at JET and AUG. J Nucl Mater. 2013;438(SUPPL):S426–S430. doi: 10.1016/j.jnucmat.2013.01.086.

[13]Loarte A, et al. Progress in the ITER Physics Basis Chapter 4: Power and particle control. Nucl Fusion. 2007;47(6):S203. doi: 10.1088/0029-5515/47/6/S04.

[14]Goldston RJ. Heuristic drift-based model of the power scrape-off width in low-gas-puff H-mode tokamaks. Nucl Fusion. 2012;52(1):013009. doi: 10.1088/0029-5515/52/1/013009.